LAPPEENRANTA UNIVERSITY OF TECHNOLOGY
FACULTY OF TECHNOLOGY
DEPARTMENT OF ELECTRICAL ENGINEERING

Oxygen adsorption on Cu(510)

The examiners of this thesis are Professor Matti Alatalo and MSc. Matti Lahti.

Lappeenranta 6.7.2007

Sami Auvinen
Punkkerikatu 1 B 3
53850 Lappeenranta
Tel. +358 40 718 6223

ABSTRACT

Lappeenranta University of Technology
Faculty of Technology
Department of electrical engineering

Sami Auvinen

Oxygen adsorption on Cu(510)

Master's thesis

2007

46 pages, 34 figures and 4 tables

Examiners: Professor Matti Alatalo and MSc. Matti Lahti

Keywords: Copper, Cu(510), Stepped surfaces, Oxygen

In this work the reactivity of the stepped Cu(510) surface is studied by using $ab\ initio$ computational methods. This is done by calculating the adsorption energies and densities of states for the oxygen atom on the potential adsorption sites on the surface. Also the adsorption of molecular oxygen is studied by calculating potential energy surfaces for the oxygen molecule approaching the potential adsorption sites on the surface. The results achieved from potential energy surfaces are also checked by molecular dynamics calculations.

Stepped metal surfaces are generally considered to be more reactive towards the oxygen because the dissociation is usually enhanced on the step edges and other defects present on stepped surfaces. There exist, however, also results that suggest the terrace area being dominant on the sticking process of dioxygen on the surface.

The adsorption on the Cu(510) surface is found to be more favoured on the terrace area for both atomic and molecular oxygen, and the adsorption energies are found to be smaller than on the smooth Cu(100) surface. Also, based on the results of potential energy surface calculations, the reactivity of the surface is found to be lower than was expected for stepped surface, alltough there is a reduction on the dissociation barrier, caused by the step edge.

TIIVISTELMÄ

Lappeenrannan teknillinen yliopisto
Teknillinen tiedekunta
Sähkötekniikan osasto

Sami Auvinen

Oxygen adsorption on Cu(510)

Diplomityö

2007

46 sivua, 34 kuvaa ja 4 taulukkoa

Tarkastajat: Professori Matti Alatalo ja DI Matti Lahti

Hakusanat: Kupari, Cu(510), Askelpinnat, Happi

Tässä työssä on tutkittu kuparin (510)-askelpinnan reaktiivisuutta käyttäen apuna kvanttimekaanisia $ab\ initio$ laskentamenetelmiä. Tutkimus on toteutettu laskemalla happiatomin adsorptioenergia ja tilatiheys erilaisissa potentiaalisissa adsorptiopaikoissa pinnalla. Myös happimolekyylin adsorptiota ja hajoamista on tarkasteltu laskemalla pintaa lähestyvälle molekyylille potentiaalienergiapintoja. Energiapintojen tuloksia on myös täydennetty kvanttimekaanisilla molekyylidynamiikkalaskuilla.

Metallisia askelpintoja pidetään yleisesti sileitä pintoja reaktiivisempina happea kohtaan, johtuen askeleen reunan pienentävästä vaikutuksesta molekyylin hajoamisen tiellä olevaan energiavaliin. On kuitenkin olemassa myös tuloksia, jotka osoittavat hapen tarttumisprosessin olevan hallitseva juuri terassialueella, askeleen reunan sijasta.

Tässä työssä on todettu hapen adsorboituvan Cu(510)-pinnalla tehokkaimmin juuri terassilla olevaan hollow-paikkaan. Myös adsorptioenergiat ovat tällä pinnalla pienempiä kuin sileällä (100)-pinnalla. Potentiaalienergiapintojen perusteella Cu(510)-pinnan todetaan myös olevan vähemmän reaktiivinen kuin askelpintojen yleisesti odotetaan olevan, vaikka askeleen reunan todetaankin pienentävän happiatomin hajoamisen esteenä olevaa energiavallia.

PREFACE

This Master's thesis has been done in Laboratory of Electronics Materials Science, in Lappeenranta university of technology, Faculty of Technology, Department of Electrical Engineering. All calculations were done by using the generous computer resources of CSC-Scientific Computing Ltd., Espoo, Finland.

I thank Professor Matti Alatalo for supervising this work, and also for advisory, support and proof-reading. I also like to thank MSc. Matti Lahti, the second supervisor of this work, and MSc. Antti Puisto for their advisory during this study.

Special thanks goes also to my wife Inka, and my son Niilo for their patience and support during my studies here in Lappeenranta. I would also like to acknowledge my parents for their support during all these years.

Lappeenranta 6.7.2007

Sami Auvinen

Contents

ABBREVIATIONS

DFT	Density Functional Theory
DOS	Density Of States
FCC	Face Centered Cubic
GGA	Generalized Gradient Approximation
HREELS	High Resolution Electron Energy Loss Spectroscopy
LCAO	Linear Combination Of Numerical Atomic Orbitals
LDA	Local Density Approximation
LEED	Low Energy Electron Diffraction
MD	Molecular Dynamics
MPS	Molecular Precursor State
PDOS	Projected Density of States
PES	Potential Energy Surface
SIESTA	Spanish Initiative for Electronic Simulations with Thousands of Atoms
STM	Scanning Tunneling Microscopy
TS	Transition State

1 INTRODUCTION

In this study the dissociation and adsorption of oxygen on Cu(510) surface is studied by using $ab\ initio$ computational methods. The dissociation and adsorption of oxygen on metal surfaces is a very common process, and it also plays a major role in many catalytic phenomena. This is because the initial stage of oxidation, dissociative adsorption, is usually the first step of these reactions.

On the metal surfaces the oxidation and corrosion is always a problem when it happens by an uncontrolled way, and because copper is widely used in electronics, the oxidation of copper surfaces has been studied in many occasions. The major reason for the interest is that oxidation affects the electrical properties of copper, and there are also many applications for controlled oxidation. These include passivation by oxidation, like growing protecting oxide layers in the manufacturing process of semiconductor devices [1].

The stepped surfaces are in the field of interest because they are usually considered to be more reactive than smooth surfaces. This can be explained by the d-band theory by Hammer $et\ al$ [2], [3]. The increased activity of the surface due to step edges makes stepped surfaces interesting from the catalysis point of view, and we should also remember that on the real surfaces there are allways steps present. This is due to the fact that the tolerance in cleaving process easily causes steps on the surfaces. There are also situations where a spontaneous facetting and step formation exists on smooth surfaces when they are annealed [4].

The main reason to choose this particular surface to be studied here was that we have already studied the oxidation of Cu(211) and Pd(211) surfaces [5], and there also exists studies of oxidation of the Cu(410) surface [6]. In this way the Cu(510) surface was a reasonable choice for a new high-index surface to be studied because relaxation of this surface had already been studied by Cohen $et\ al$ [7], and on Cu(510) the step also runs in the same direction as the steps in the experiments of Hirsimäki $et\ al$ [8]. From the computational point of view the Cu(510) surface also has a reasonable size of a computational supercell.

2 BACKGROUND THEORY AND EARLIER STUDIES

In this section the theory related to basic definitions is presented along with some earlier results. In the first part we will go through the definitions of the surface structures, and on the second and third part we take a brief look at the properties of surfaces, and the earlier results for oxidation of selected stepped surfaces.

2.1 Definition of lattice planes

The basic form of condensed matter is a crystalline structure, which can be specified by the *Bravais lattice*. Bravais lattice is an infinite array of discrete points, which are oriented so that the lattice looks exactly the same when viewed from whichever point in the array. The atomic positions in three dimensional Bravais lattice are determined by the position vector

$$\mathbf{R} = n_1\mathbf{a}_1 + n_2\mathbf{a}_2 + n_3\mathbf{a}_3, \tag{1}$$

where $\mathbf{a}_1$, $\mathbf{a}_2$ and $\mathbf{a}_3$ are any three vectors called *primitive vectors*, and n_1, n_2 and n_3 are integers. [9].

Copper has the monoatomic *face-centered cubic* (FCC) Bravais lattice, which is shown in figure 1, and for a FCC lattice the primitive vectors can be formed as

$$\mathbf{a}_1 = \frac{a}{2}(\hat{\mathbf{y}} + \hat{\mathbf{z}}), \mathbf{a}_2 = \frac{a}{2}(\hat{\mathbf{z}} + \hat{\mathbf{x}}), \mathbf{a}_3 = \frac{a}{2}(\hat{\mathbf{x}} + \hat{\mathbf{y}}). \tag{2}$$

The constant *a* in equation 2 is 3.16 Å in the case of copper. [9]

Bravais lattice actually defines an infinite bulk of material, and when we consider real surfaces we will have to restrict it to some finite extend. When a real surface is formed, the bulk has to be cleaved somehow, and the crystallographic direction of the cut actually defines the surface being constructed. The definition of surfaces is done by using the *Miller indices*, (*hkl*), which actually tell you along which crystallographic plane the surface is cleaved. Miller indices refer to the shortest reciprocal lattice vector, which is normal to the plane, and is given by [9]

$$\mathbf{k} = h\mathbf{b}_1 + k\mathbf{b}_2 + k\mathbf{b}_3. \tag{3}$$

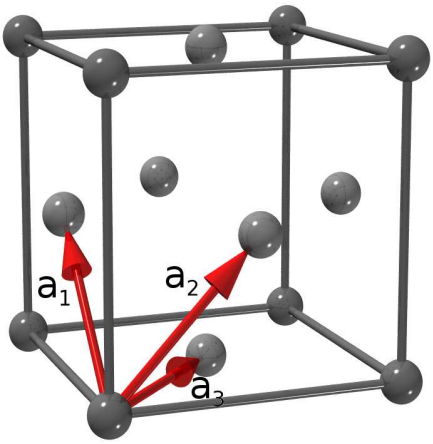

Figure 1: Some points of the face-centered cubic (FCC) Bravais lattice, and the primitive vectors forming the lattice.

In equation 3, reciprocal primitive vectors $\mathbf{b}_i$ are defined by

$$\mathbf{b}_1 = 2\pi \frac{\mathbf{a}_2 \times \mathbf{a}_3}{\mathbf{a}_1 \cdot (\mathbf{a}_2 \times \mathbf{a}_3)}, \mathbf{b}_2 = 2\pi \frac{\mathbf{a}_3 \times \mathbf{a}_1}{\mathbf{a}_1 \cdot (\mathbf{a}_2 \times \mathbf{a}_3)}, \mathbf{b}_1 = 2\pi \frac{\mathbf{a}_1 \times \mathbf{a}_2}{\mathbf{a}_1 \cdot (\mathbf{a}_2 \times \mathbf{a}_3)}, \tag{4}$$

where primitive vectors $\mathbf{a}_i$ are defined by equation 2. [9]

2.2 Stepped surfaces

When we consider the surfaces defined by the Miller indices, we can separate them in two different categories based on the absolute values of the indices (*hkl*): Low index surfaces and high index surfaces. When all three indices have an absolute value equal to one or zero, the resultant surface is smooth and and it is called a low index surface. When any of the indices have bigger absolute values, the resultant surface is referred as a high index surface, and these are often stepped. Few examples of low index surfaces are (100), (110) and (111) surfaces, and three examples of high index surfaces are (211), (410) and (510) surfaces.

Stepped surfaces that are only slightly misaligned from a low index plane are called *vicinal surfaces* [10]. A vicinal surface is constructed by joining together low index surfaces separated by a monoatomic steps. On these surfaces the smooth area between the steps is called terrace, while the small plane between the step and terrace is called microfacet.

For FCC structure the (510) and (410) surfaces for example, have (100) terraces and (110) microfacets, while (211) surface has (111) terraces and (100) microfacets.

Stepped surfaces are often considered to be less stable when compared to smooth low index surfaces. This is due to higher surface energy on stepped surfaces, and it causes a tendency of the stepped surfaces to flatten out. In ref. [11] D. Spišák has calculated the surface energies and step the formation energies for Cu(100) vicinal surfaces, including the Cu(510) surface, which is rotated by 11.3 degrees away from the [100] direction [11]. Spišák found the surface energy of E=3.40 eV per surface atom for relaxed Cu(510), which is quite large when compared to E=0.596 eV per surface atom for Cu(100) [11]. The higher surface energy of (n11) and (n10) metal surfaces predicts a reduction of step heights and contraction of topmost surface layer distances. These two phenomena can be seen from relaxation patterns for these surfaces [7], [12].

For FCC crystals, (n10) vicinal surfaces have (100) terraces and the step atoms are next nearest neighbors to each other [11]. When (100) terraces are the second most close packed ones after (111) structures, and also the (110) microfacet represents quite open structure, we can conclude that steps on Cu(n10) vicinal surfaces are not close packed. This leaves more open bonds on the steps, and it usually causes the center of the d-band to shift into higher energy levels [13]. According to the d-band theory [2], [3] this upshift would predict these surfaces to be quite reactive towards molecular adsorbates.

The unstable Cu(100) vicinal surfaces are also known to become stable by reconstruction when they are exposed to oxygen, like in case of Cu(511) when it transforms to {410}and {311}facets upon oxygen adsorption [14]. This tendency of some of the Cu(100) vicinals to facet to {410}under oxygen exposure has been studied by Knight $et\ al$ [4]. They concluded that this strong energetic favouring of <100> step-edges under oxygen exposure is linked to formation of Cu-O-Cu-O chains, which is the stable element when Cu(100) and Cu(110) surfaces reconstruct under oxygen exposure [4].

2.3 Molecules on stepped surfaces

The effect of steps on the metal surfaces has been studied by using many different methods, both theoretical and experimental. These methods include different density functional theory (DFT) based calculation packages, scanning tunneling microscopy (STM), X-ray diffraction, high resolution electron energy loss spectroscopy (HREELS) or low energy electron diffraction (LEED), just to mention a few of them. The results achieved for stepped surfaces by these methods seem to be quite coherent with each other, showing the stepped surfaces to be more reactive than smooth ones.

As a first example, Xu and Mavrikakis [13] have studied the effect of steps to O_2 dissociation on Cu(211) surface by using DFT based computational methods. Their results show that the steps enhance the dissociation of O_2, when from the six studied trajectories two were molecular precursors, and rest of the trajectories exhibited direct dissociation of O_2. They also found that these molecular precursors found near the step foot are more favourable than corresponding ones on the flat Cu(111) surface, so that the initial and transition states are stabilized by 0.5 eV. Also for atomic the oxygen the threefold sites near the foot of the step were more favourable than the less coordinated sites on the terrace, and the surface-adsorbate interaction in case of dioxygen appears to be stronger on the foot of the step. This was seen in spontaneous dissociation of O_2 on the foot of the step. Their final conclusion was that this enhanced activity of the foot of the step is a consequence of this area being more electron-rich than the edge of the step due to the charge density smoothing. They also figured that this enhanced precursor dissociation is mainly a result of stabilizing effect of steps to these precursor states, and lowered activation barriers. [13]

Based on their own studies and those of Chorkendorf and co-workers on N_2 dissociation on Ru(0001) [15], [16], and on O_2 adsorption on clean and modified Cu(100) [1], Xu and Mavrikakis confirmed also that the effect of steps to molecule dissociation is more pronounced on Ru surfaces than on Cu surfaces [13]. This was shown when the rate of N_2 dissociation on Ru(0001) is reduced by nine orders of magnitude when the surface is dosed with a small amount of Au atoms, which effectively adsorb on the steps and other defects on Ru surface, thus blocking oxygen adsorption on these sites [13], [15], [16]. When the same thing is tested on O_2 on Cu(100) dosed with Ag, which does the same thing for steps and defects as Au on Ru surfaces, the sticking probability is decreased, but the decrease remains smaller than on Ru surfaces [13], [1].

In another study, this origin of enhancement of the dissociativity, suggested by Xu and Mavrikakis [13], was confirmed by Šljivančanin and Hammer [17], who found the enhanced dissociativity of O_2 due to Pt steps in DFT studies, and came up with the same origin for the phenomenon. Šljivančanin and Hammer saw that chemisorption and dissociation of O_2 is favoured on Pt(221) and Pt(211) steps rather than terraces, and after the dissociation the atomic oxygen also binds about 0.4 eV more tightly to steps than terraces. [17]. To go more in detail, the d-band center of the step atoms is shifted 0.45 eV up, and the chemisorption potential energy is about 0.8 eV lower, and according to the d-band theory suggested by Hammer $et\ al$ earlier [2] [3],they explained this enhancement in reactivity by stronger adsorbate-surface interaction due to higher energy of d-states [17].

In agreement with the results of Xu and Mavrikakis [13], Šljivančanin and Hammer saw that molecular precursor states (MPS) are more stabilized by high-energy d-band center than the dissociation transition state (TS) [17]. What is interesting is that they also found that the dissociation barrier from MPS goes higher as the adsorption site comes more undercoordinated, thus leading to about 0.3 eV higher dissociation barriers on the step sites [17]. This would seem to suggest that steps actually lower the reactivity of the surface, but Šljivančanin and Hammer noted, however, that the dissociation barrier from the gas phase level is 0.5 eV smaller on Pt steps than it is on flat Pt(111). This way they concluded, according to the earlier studies by them and co-workers [18], that this direct dissociation enhanced by steps would dominate the reaction kinetics [17].

If we like to compare more results on the different stepped transition metal surfaces, we might also discuss the results achieved by M. Lahti $et\ al$ on oxidation of Pd(211) and Cu(211) surfaces [5]. Lahti $et\ al$ used DFT based static potential energy surface (PES) calculation complemented with the first principles molecular dynamics (MD), and found steering effects that complicate the dissociation dynamics of O_2 on stepped surfaces [5]. The conclusion of their study was that on both Pd(211) and Cu(211) surface there is no early barrier for molecular sticking and these surfaces are highly attractive for incoming oxygen molecules [5]. On both materials the adsorbed oxygen molecules favor the (100) microfacet's hollow site,where the dissociation is enhanced by steps, but the actual step edge does not seem to be particularly reactive [5]. This kind of phenomenon is also observed in this study on the (110) microfacet and step edges of Cu(510), but on different energy scale, as seen later in the results section.

If we consider earlier studies on oxidation of high index surfaces, one example would be the study of Vattuone $et\ al$ on O_2 on Cu(410) [6]. In their studies Vattuone $et\ al$ have

used the supersonic molecular beams to investigate the energy and angle dependence of the initial sticking probability, S_0, for O_2. Their results show that over the investigated temperature range, meaning temperatures from 127 K - 800 K, the adsorption occurs dissociatively. At thermal beam energy S_0 depends on crystal temperature only below 150 K, where S_0 decreases from 0.4 to 0.2. At the hyperthermal energies S_0 is independent of the crystal temperature. [6]

Just like in all earlier studies, Vattuone $et\ al$ [6] also concluded that low coordination sites at steps cause a reduction on the activation energy for indirect dissociation, thus resulting a higher dissociation probability. The sticking probability was also seen to be affected by the limited width of the nanoterasses, which they also found to be less active than extended ones. The presence of steps on Cu(410) increases the reactivity of Cu(100) at low impact energies for oxygen molecule, but on hyperthermal energies oxygen adsorption is globally reduced due to lower reactivity on the terraces, which compensates the effect of steps. [6] The same kind of reduction on terrace activity due to limited terrace width was also reported by Savio $et\ al$ in their studies on O_2 dissociation on Ag(410) [19].

Altough the general trend in results for most of the stepped metal surfaces indicates increased reactivity due to steps, there are also some opposing opinions. Uesugi-Saitow and Yata [20] have studied the effect of the tensile stress to the dissociative chemisorption of O_2 on clean and O-covered Cu(100), by using supersonic molecular beam techniques and LEED. Their results show that initial dissociative sticking probability, S_0, for O_2 on clean Cu(100), increases with higher translational energies for incoming O_2 reaching a final value of about 0.8. Their conclusion was that a direct activated dissociation process is dominant for the dissociative adsorption, and the sticking process would actually dominate on terraces rather than on steps or other vacant sites. [20], [21]

3 COMPUTATIONAL METHODS

After the background briefing in the last chapter, we will go through the methods used in this study. In the first part we deal with the theoretical issues, and on the second part we cover the practical details of calculations.

3.1 Basic theory

In this section we cover briefly the theoretical tools needed in calculations, and the rest of the section is arranged as follows. First we will see the basics about the density functional theory, which pretty much is the key element behind all these calculation done for this thesis. After that we will go through the basics of pseudopotentials and potential energy surfaces needed in calculations.

3.1.1 Density functional theory

Density functional theory is based on the simple idea that any property of the system of interacting particles can be handled as a functional of the ground state density $n_0(\mathbf{r})$. The original method behind DFT was proposed by Thomas [22] and Fermi [23] in 1927, but since it has been further developed by others. [24]

The original Thomas-Fermi method approximates the kinetic energy of the system as an explicit functional of the density, which is idealized as non-interacting electrons in homogeneous gas, having density equal to the local density at that point. Originally Thomas and Fermi neglected the exchange and correlation among the electrons, but this was later implemented by Dirac [25]. This gives us the functional for energy for electrons in an external potential V_{ext}**(r)**

$$\begin{aligned} E_{TF}[n] = (\frac{3(3\pi^2)^{\frac{2}{3}}}{10}) \int d^3r n(\mathbf{r})^{5/3} + \int d^3r V_{ext}(\mathbf{r}) n(\mathbf{r}) \\ + (-\frac{3}{4}(3/\pi)^{\frac{1}{3}}) \int d^3r n(\mathbf{r})^{4/3} + \frac{1}{2} \int d^3r d^3r' \frac{n(\mathbf{r}) n(\mathbf{r}')}{|\mathbf{r} - \mathbf{r}'|}. \end{aligned} \tag{5}$$

In equation 5 the first term corresponds to the local approximation to the kinetic energy, the third term is the local exchange and the last term is the Hartree energy. As obvious, the ground state can be found by minimizing the E[n] for all possible n**(r)**. Altough the Thomas-Fermi method gives the idea how DFT works, it is way too inaccurate for present day electronic structure calculations. [24]

Two basic theorems on which the modern DFT is based on, were proposed by Hohenberg and Kohn [26], and the idea behind these theorems was to formulate DFT as an exact theory of many-body systems. The first of these theorems states that if we have a

system of interacting particles in external potential V_{ext}(**r**), the external potential V_{ext}(**r**) is uniquely determined by the ground state density n_0(**r**). The second theorem states that for any external potential V_{ext}(**r**), can be defined a universal functional for energy E[*n*] in the terms of density n(**r**), and by finding a global minimum for E[*n*] as a function of n(**r**), we can find the exact ground state and the ground state density. The energy functional can be formulated as

$$E_{HK} = T[n] + E_{int}[n] + \int d^3 r V_{ext}(\mathbf{r}) n(\mathbf{r}) + E_{II}, \tag{6}$$

where $T[n]$ represents the internal kinetic energy, $E_{int}[n]$ represents the internal potential energy, and the E_{II} is the interaction energy of the nuclei. [24]

The key element that has made DFT the most used method for electronic structure calculations was introduced in 1965, and it is the Kohn-Sham ansatz. Kohn and Sham found that it is possible to replace the original, rather complicated many-body problem with an auxiliary independent-particle problem, which is far more easily solved. The Kohn-Sham method is self-consistent, and it involves independent particles and interacting density. [24]

The Kohn-Sham ansatz is based on two assumptions, the first one being that the exact ground state of the system can be represented by the ground state of the auxiliary system of non-interacting particles. This assumption, however, has not been proved for for the real systems, but still the method gives reasonable results for real systems.The second assumption is that the auxiliary Hamiltonian is selected so, that it has a usual kinetic operator and an effective local potential V^{σ}_{eff}(**r**), which acts on the electron in the point **r**, having a spin of σ. [24]

By this Kohn-Sham approach, we can rewrite the Hohenberg-Kohn expression (equation 6) in the form

$$E_{KS} = T_s[n] + \int d\mathbf{r} V_{ext}(\mathbf{r}) n(\mathbf{r}) + E_{Hartree}[n] + E_{II} + E_{xc}[n], \tag{7}$$

where T_s[*n*] is the kinetic energy functional, $E_{Hartree}$[*n*] is the classical Coulomb interaction energy of the electron density interacting with itself, E_{II} is the interaction between the nuclei, V_{ext}(**r**) is the external potential due to the nuclei and any other external fields, and E_{xc}[*n*] is the exchange-correlation energy, which includes all many-body effects. [24]

In any practical implementation the accuracy of DFT is strongly dependent on the accuracy of the exchange-correlation functional [10]. Since the exchange-correlation energy is not generally known, the exchange-correlation functional remains also exactly underived. To overcome this problem, number of different approximations have been developed, the most common being the *Local Density Approximation* (LDA), where the exchange-correlation energy is approximated by the exchange-correlation energy of the homogeneous electron gas [10].

The problem with the LDA is that it shows overbinding, and the cohesive energies are too large [10], and to overcome this, more efficient approximations have been developed. The Generalized Gradient Approximation (GGA) includes also the gradient of the density in exchange-correlation energy, and leads to better results. Still, despite the improvements of GGA, there are problems with the accuracy of DFT calculations [10].

3.1.2 Pseudopotentials

In any practical implementation of DFT, the computational load is significantly increased with the amount of electrons included in calculations [10]. This problem can be overcome by the taking into account the fact that most of the chemical and solid-properties are determined only by the valence electrons, so we can neglect the effect of the core electrons [10].

In order to lower the computational demands, this idea has been developed in the form of *pseudopotentials*. In the pseudopotential approach, the original potential is replaced with the one neglecting the effect of the core electrons, thus having almost the same properties, but causing much lower demands for computational power [10]. Inside the core radius the pseudopotential and the corresponding wavefunction should be as smooth as possible, and this property is referred to as the softness of the pseudopotential [10]. Outside the core radius the pseudopotential should be effectively identical to the real potential to describe the long range interactions correctly, and it should also conserve the norm of the real potential [10].

The actual pseudopotential can be constructed many different ways, and the scheme used, and the required softness of the pseudopotential depend on the application on which the potential is used for. The most commonly used generation schemes for pseudopotentials

are developed by Bachelet, Haman and Schlüter [27], and Troulier and Martins [28], [29], and especially the Troulier-Martins pseudopotentials are constructed to be particularly soft [10].

3.1.3 Potential energy surfaces

The potential energy surface (PES) is an important tool in analyzing the adsorption of molecules or atoms on surfaces. The PES represents the energy hyperplane over the space of atomic coordinates of the involved atoms, and it gives direct information about adsorption sites and energies, and the existence of barriers for adsorption [10]. In reality the PES is 6-dimensional, corresponding to all atomic coordinates, but in practical representations we must restrict the dimension used. This is partly due to problems in presenting the multidimensional plots, but the major reason is the computational demand. When the number of dimensions used is raised, also the number of sample points in the space is raised. Because of this limitation the PES plots calculated here are only two-dimensional cuts from the real PES.

One note of caution is that these two-dimensional cuts can be misleading due to information loss when the sample set of the energy space is chosen. When these PES plots are analyzed we see only a portion of the real energy plane, and cannot be sure about the form of the energy surface in the other direction. This is why results achieved with PES plots should be checked by using other methods, such as molecular dynamics (MD).

3.2 Computational details

All calculations in this work have been done by using the Spanish Initiative for Electronic Simulations with Thousands of Atoms -package (SIESTA), a computer program package, that uses Kohn-Sham self consistent density functional method with LDA or GGA to perform electronic structure or $ab\ initio$ simulation calculations [30]. Other features of SIESTA are that it uses norm-conserving pseudopotentials, and linear combination of numerical atomic orbitals (LCAO) as the basis set. In this way the basis set is general and very flexible, and the atomic orbitals are numerical in shape [30].

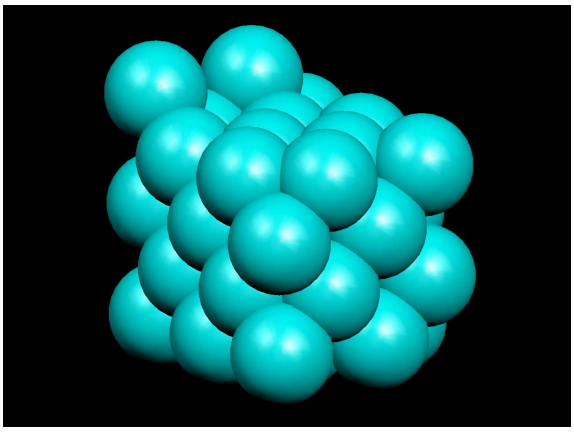

Figure 2: The Cu(510) supercell used in the calculations.

3.2.1 The supercell

In SIESTA simulations the surface is constructed by tiling it up from a piece called the supercell. The supercell can be considered as a unit cell of the surface, and during the simulations this supercell replicated to fill all of the infinite space in the simulation model. In these calculations the Cu(510) surface was constructed with a supercell of four Cu atom layers and one atom high step. There are ten copper atoms in each layer and the step is constructed of two atoms, so the final count for Cu atoms used is 42. The experimental lattice constant for copper is a=3.61 Å but here we used a bigger lattice constant a=3.695 Å, which suites better for these computational methods. The structure of the supercell is shown in figure 2.

To achieve more accurate results, the number of layers should be at least four, like we used here. Also the width of the supercell affects to the distance between adjacent oxygen atoms or molecules on the surface. This is because not only the surface element but also the adsorbating oxygen over the surface is replicated, and instead of one oxygen molecule or atom we have a “chain” of them approaching the surface. The problem here is, that increasing the width or height of the slab rapidly increases the amount of atoms needed in the supercell, and thus increases the demand for computational power and memory capacity. For this reason the number of layers and width of the supercell are compromises between the accuracy and computing load. In this case the amount of 42 atoms was seen sufficient and reasonable.

Table 1: Tested K-point meshes and corresponding total energies of the relaxed clean Cu(510) surface.

K-points	Tot.energy [eV]
$2 \times 3 \times 1$	-65171.14
$2 \times 4 \times 1$	-65170.94
$5 \times 6 \times 1$	-65171.03
$5 \times 7 \times 1$	-65171.01
$6 \times 7 \times 1$	-65171.01
$6 \times 8 \times 1$	-65171.01
$8 \times 9 \times 1$	-65171.02
$8 \times 10 \times 1$	-65171.00
$9 \times 10 \times 1$	-65170.10
$9 \times 11 \times 1$	-65171.00

3.2.2 K-points

One of the most important parameters that needs to be set for calculation is the K-point mesh. The K-point mesh is used to sample the Brillouin-zone in K-space so, that the first Brillouin-zone is divided according to the selected K-point mesh.

In these calculations we used the Monchorst-Pack -scheme [31], where the K-points are homogeneously spaced over the Brillouin-zone. From all of these points only the irreducible ones are used in the calculations. The selected K-point set affects the convergence of the total energy of the system, so a few test calculations were done in order to select a set that is large enough for these calculations. The results of these tests are shown in Table1.

Based on the results of the test calculations, the $9 \times 10 \times 1$-sampling was selected for the atomic oxygen calculations. With this sampling set the amount of irreducible points was 50. Later, for the PES and MD calculations, the $6 \times 7 \times 1$-set was selected in order to lower computational demands. With this smaller set the total energy is almost identical to the previous one, and the amount of irreducible K-points is only 24.

4 RESULTS

In this part of the text we present the actual results of the calculations. The results are presented in chronological order, starting from the relaxation of the surface. After the relaxation results the results concerning the adsorption of atomic and molecular oxygen are presented in corresponding order. In the final subsection we give the information about the results gained from the molecular dynamics calculations.

4.1 Relaxation

The first step of these calculations was to relax the ideal clean surface. The relaxation was done using the conjugate gradient method in the calculation of atomic forces, and during the relaxation the positions of the atoms in the bottom layer were kept fixed, while other atoms were allowed to move.

The results show small changes in atomic positions, and when compared to the ideal {100}interlayer distance 1.8475 Å, the step edge on the relaxed surface is 1.82% lower and it has moved also about 0.35% closer to the next atom row on the upper terrace. While the step edge is lowered in contrast to the terrace, the distances between {100}atomic layers have generally become bigger so that average values are $d_{23} = +4.74\%$, $d_{34} = +5.54\%$ and $d_{45} = +3.04\%$. Schematic pictures of relaxation of atomic layers and rows are in figures 3 and 4.

The changes in Cu-Cu nearest neighbor bonding lengths after relaxation are depicted in figure 5. These changes are proportional to the ideal Cu-Cu bonding length of 2.613 Å. As an average the bonding lengths are 1.16 $\%$ longer after the relaxation.

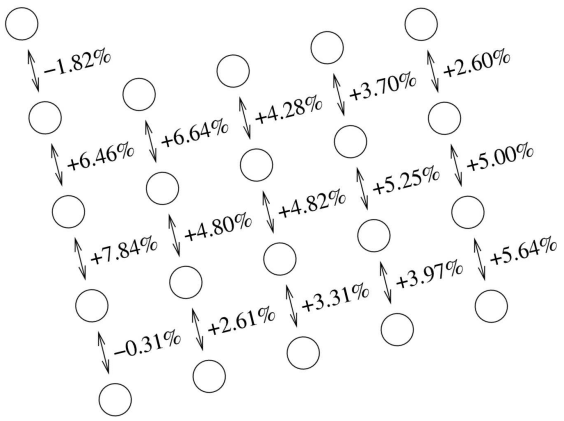

Figure 3: Relative changes in interlayer distances between atom rows on Cu(510) after the relaxation. Numbers are relative to the ideal {100}interlayer distance 1.8475 Å.

When these results are compared to those achieved by D. Spišák [11] for Cu(105) surface, we find out that the inward/outward -relaxation scheme is quite similar, altough the individual bonding length changes are a bit different. This difference, however, is probably due to different amount of layers used in these calculations, when Spišák [11] has used 10 layers instead of four used here. Spišák has also used the different Cu lattice spacing, a=3.637 Å, which is smaller than the one used in these calculations. Also the relaxation method is different in these calculation, when Spišák has allowed both the upper- and lower side of the slab to relax, while the middle layer of the slab was kept fixed.

In theory for relaxation of metal surfaces, given by A. Groß [10], the Smoluchowski charge smoothing in atomic structure leads in reduction of first inter-layer spacing [10], [32], [33]. When the first atomic layer becomes nearer the second one, there is a charge accumulation in other layers, and this charge accumulation leads to outward relaxation of the other layers [10]. As we can see from figures 3-5, we see that this theory seems to be in agreement with the results. Clearly there exists a reduction on step height and first interlayer spacing, while other layers exhibit an outward relaxation. Also a tendency for the surface to flatten can be seen from the relaxation results in figures 3-5.

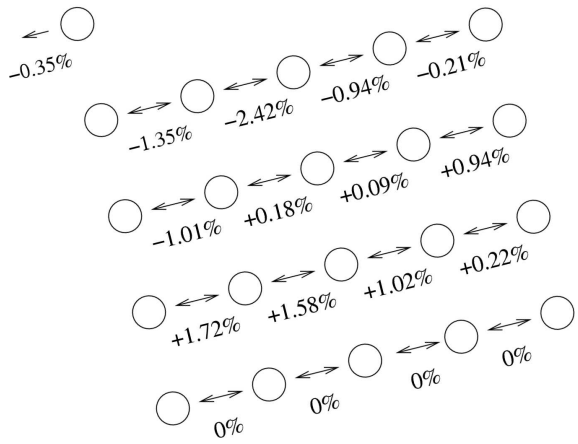

Figure 4: Relative changes in interlayer distances between atom rows on Cu(510) after the relaxation. Numbers are proportional to the ideal {100}interlayer distance 1.8475 Å.

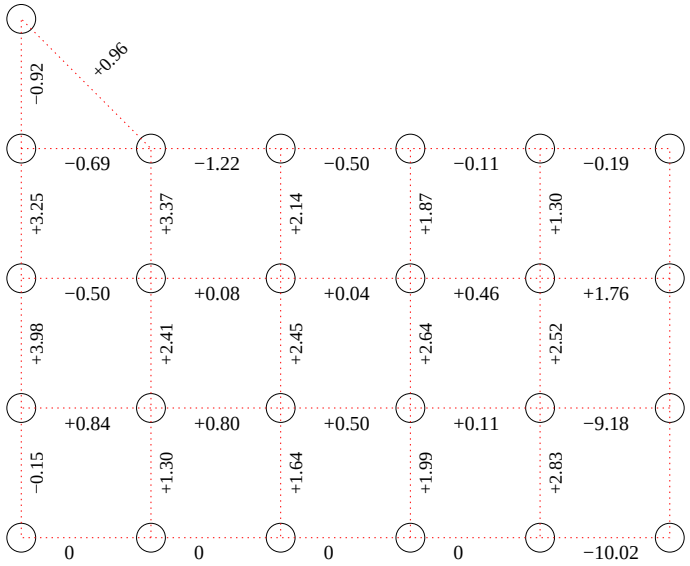

Figure 5: Relative changes in Cu-Cu nearest neighbor bonding lengths after the relaxation. Changes are proportional to the ideal bonding length of 2.613 Å, before the relaxation.

4.2 Total energy of the oxygen atom

For the calculation of the adsorption energy of an oxygen atom on the surface we needed to know the energy of a single oxygen atom. In order to find out this energy, SIESTA was used to relax a single oxygen molecule in vacuum. In this single calculation the K-point mesh was set to be $2 \times 2 \times 2$, and the supercell dimensions were automaticly set up by SIESTA. Also the energy of one oxygen atom was calculated with the same parameters, in order to find the bonding energy of the oxygen molecule.

The results show -884.23 eV for the total energy of oxygen molecule, and the bonding length of 1.24 Å, while the bonding energy was found to be 6.59 eV. By dividing the energy of the molecule by two, we have the total energy of -442.12 eV for the oxygen atom. The bonding length corresponds reasonably well to the experimental value 1.207 Å [34], but the bonding energy is overestimated, the real one being only 5.08 eV. This overestimation, however, is not a surprise when GGA is used for approximation of exchange-correlation energy.

4.3 Adsorption of atomic oxygen

To begin with the study of oxidation of the Cu(510) surface, the adsorption of atomic oxygen was studied on the surface. This was done by calculating the adsorption energies and *Density of States* (DOS) for oxygen atom on the surface.

4.3.1 Adsorption energies

To find out the adsorption sites on the surface, the adsorption energy of the oxygen atom on different sites on the surface was calculated. Eleven different sites were selected for this purpose, and these sites were selected according to the previous studies [1], [5], [13], [19], [20], [35], and they cover all the interesting and potential adsorption sites near the step edge, and on the terrace.

The selected sites are presented in figure 6. Site one is the hollow site on the step edge. Site two is the hollow site next to the step edge on the upper terrace, while site three is

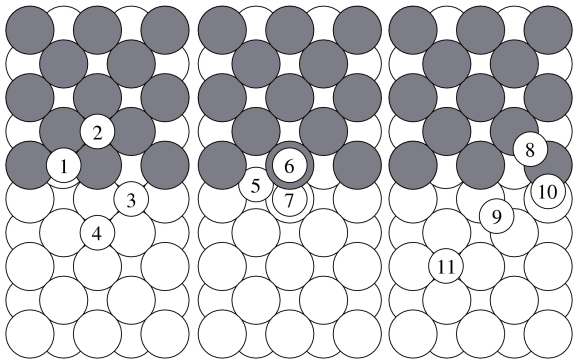

Figure 6: The selected adsorption sites for atomic oxygen on Cu(510) surface.

the one on the lower terrace. Site four is the hollow site one atom row away from the step on the lower terrace, site 11 represents the hollow site in the middle of the (100) terrace, and site five is the one on the (110) microfacet. Sites six and seven are the top sites on the step edge and below it, and the sites eight, nine and ten represent the bridge sites next to the step edge, below it and on the (110) microfacet, in corresponding order.

The results for the adsorption energies are presented in Table 2. The table gives the total energy of the system, and the adsorption energies for oxygen on different sites. The adsorption energy is calculated by using the equation

$$E_{ads} = E_{system} - (E_{atom} + E_{surface}), \tag{8}$$

in which E_{ads} is the adsorption energy, E_{system} is the total energy of whole system, E_{atom} is the energy of the oxygen atom and $E_{surface}$ is the total energy of a clean relaxed surface. In the calculations $E_{surface}$ was set to be -65170.10eV according to $9 \times 10 \times 1$ -mesh, and E_{atom} was set to be -442.12 eV as it was calculated earlier.

In Table 2, the energies left empty correspond to these sites being unstable. In these cases the oxygen atom did not stay in the place where the energy was originally intended to be calculated during the relaxation. Even tough we are unable to calculate the adsorption energy, we can conclude that these sites are not local or global energy minima, and so they are not the potential adsorption sites during the oxidation process.

Table 2: The total energies of the system and the adsorption energies of oxygen for calculated adsorption sites. The most reactive (lowest adsorption energy) site is the hollow site at the (100) terrace. The numbering of the sites refers to picture 6. The empty energies refer these sites to be unstable, so the calculation of adsorption energies was impossible.

Ads.site	Tot.energy [eV]	Ads. energy [eV]
1	-65614.43	-1.31
2	-65614.45	-1.33
3	-65614.13	-1.01
4	-65614.42	-1.31
5	-65614.12	-1.00
6	-	-
7	-	-
8	-	-
9	-	-
10	-65613.59	-0.47
11	-65614.55	-1.43

As we can also see from Table 2, the most favourable adsorption site is the fourfold hollow site in the middle of the (100) terrace. This result is not surprising because it is known that fourfold hollow sites are the most favourable adsorption sites for atomic oxygen on several surfaces [5], [35], but what is worth noticing is that the presence of the step does not seem to enhance the adsorption energy on the step edge.

Also the magnitude of adsorption energies on the Cu(510) surface is smaller than on the smooth Cu(100) surface. A. Puisto has previously calculated the adsorption energies of atomic oxygen on the Cu(100) surface, and he found that the highest adsorption energy is -2.42 eV on the fourfold hollow site, while the lowest adsorption energy is -0.57 eV on the top site [35]. So in this case the adsorption of oxygen seems to be slightly reduced on the Cu(510) surface.

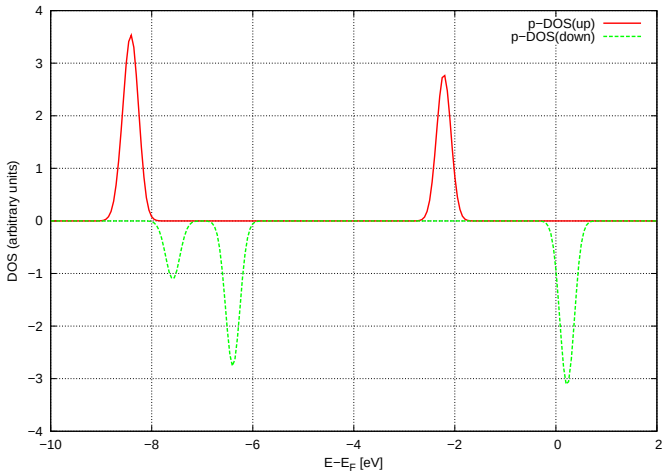

Figure 7: Projected p-DOS for an oxygen atom in vacuum.

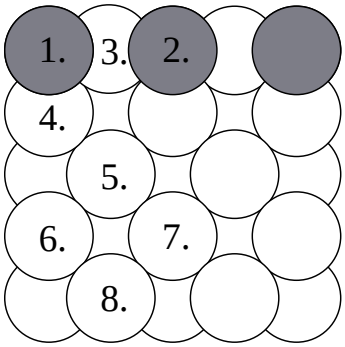

Figure 8: Selected Cu atoms on clean (510) surface. The gray circles represent the step edge atoms while the white circles represent the atoms on the lower terrace.

4.3.2 Density of states

In order to see the electronic behavior in the adsorption of atomic oxygen, the *projected density of states* (PDOS) were calculated for oxygen atom, selected copper atoms on clean Cu(510) surface and for a few atoms on the most interesting adsorption sites. In figure 7 we can see the projected p-DOS for the oxygen atom in vacuum. The p-DOS in figure 7 corresponds well to the energy level diagram for O_2 [36], and for the p-DOS figures for oxygen calculated by M. Lahti in his Masters' thesis [37].

On the clean surface, the PDOS figures were calculated for a few selected surface Cu atoms. The representative Cu atoms were selected around the four most favourable adsorption sites for atomic oxygen, so we can compare those with the ones calculated after the adsorption of the oxygen atom. The selected Cu atoms are depicted in figure 8.

Table 3: The centers of the d-band for the selected Cu atoms on the clean surface. The numbering of the atom refers to figure 8. The energy E_{cdb} is the center of the atoms d-band.

Atom	E_{cdb} [eV]
1	-1.79
2	-1.79
3	-2.35
4	-2.03
5	-1.95
6	-1.95
7	-1.95
8	-1.95

The calculated d-DOS figures for Cu atoms on the clean surface are presented in figures 9-12. In these figures the center of the d-band is also marked with a blue line, and to make the results more clear, the centers of the d-bands for the clean surface are also shown in Table 3.

As we can see from the figures 9-12, and from Table 3, the step edge moves the center of the d-band higher in the energy, and closer to the Fermi energy, which is 0 eV in these figures. It is clear from Table 3, that the atoms on the step edge (atoms one and two) have identical centers of the d-band. Also the shape of the d-DOS is identical for both of them, and it is represented in figure 9. Also the terrace atoms (5-8) have almost identical d-DOS, which is presented for the copper atom number five in figure 12. This indicates that the occupation of the d-band is quite identical for the terrace atoms.

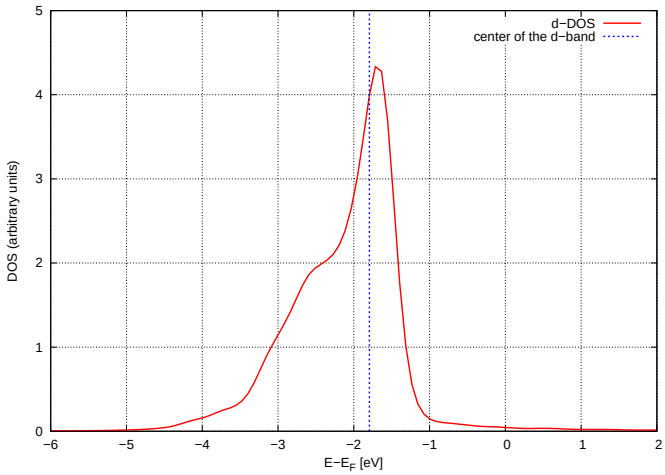

Figure 9: Projected d-DOS for the Cu atom number one on the clean surface. The blue line shows the center of the d-band. Projected d-DOS for the copper atom number two is also identical to this one here.

According to the d-band theory by Hammer $et\ al$ [2], [3], one would expect the step edge to be the most favourable adsorption region, as we see from the figure 9, but in this case it is the hollow site in the middle of the terrace which is the most favourable. This could be explained by taking a closer look at the d-DOS of the copper atoms number three and four in figures 10 and 11. In these figures the center of the d-band is again lower, so the average value of the d-band center on the step edge region is effectively lower than figure 9 alone would indicate.

In figure 13 is the total p-DOS for oxygen atom on the site number one, and the total d-DOS for the nearest copper atom, Cu number eight. As we can see, there is a clear interaction between those, and when we compare the d-DOS of the copper atom number eight to the one on the clean surface (figure 12), we see a clear enhancement in d-band occupation. The center of the d-band is now E_{cdb}=-1.98 eV, which is 0.03 eV lower than it was on the clean surface.

In figure 14 we see the total p-DOS for oxygen atom on the site number one when compared to the total d-DOS for the second nearest copper atom, Cu number one. Here we see the same changes, and the center of the d-band is E_{cdb}=-1.90 eV, which is 0.11 eV lower than it was on the clean surface.

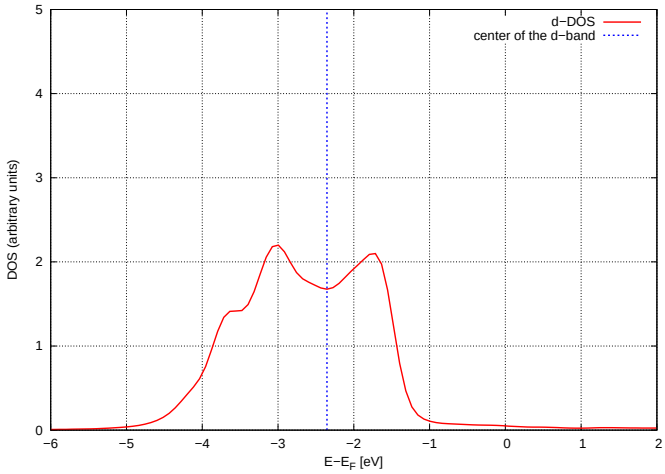

Figure 10: Projected d-DOS for the Cu atom number three on the clean surface. The blue line shows the center of the d-band.

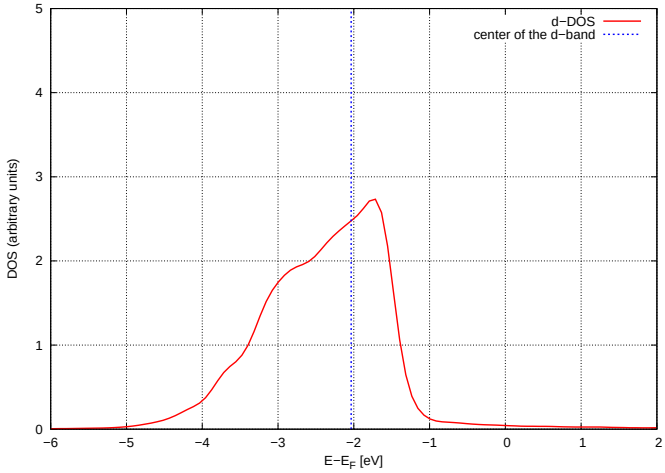

Figure 11: Projected d-DOS for the Cu atom number four on the clean surface. The blue line shows the center of the d-band.

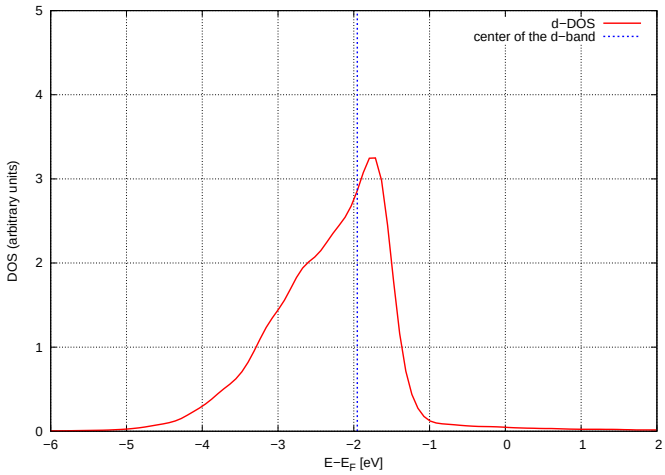

Figure 12: Projected d-DOS for the Cu atom number five on the clean surface. The blue line shows the center of the d-band. Projected d-DOS for copper atoms six, seven and eight is also identical to the one presented here.

The DOS figures for the adsorption site number two are depicted in figures 15 and 16. Also in this case there is clear interaction between the p-states of oxygen and the d-states of the copper, and the d-band occupation is also enhanced. The center of the d-band of the nearest copper atom (Cu 2) is E_{cdb}=-1.79 eV, so there is no change in it when compared to the one on clean surface. For the second nearest copper atom (Cu 8) the center of the d-band is E_{cdb}=-2.03 eV, being 0.08 eV lower than on the clean surface.

On the adsorption site number four, we see from figures 17 and 18, that the effect between oxygen atom and the nearest and the second nearest copper atoms (Cu 7 and Cu 5 respectively) are almost identical. Also the center of the d-band is E_{cdb}=-2.07 eV, being 0.12 eV lower for both the nearest and the second nearest Cu atoms.

What it comes to the most favoured atomic adsorption site, the site number 11, we see from the figures 19 and 20, that there is a small difference between d-band occupation on the nearest and the second nearest copper atoms (Cu 6 and Cu 8 respectively), but the center of the d-band is E_{cdb}=-2.08 eV, which is 0.13 eV lower, for both of them.

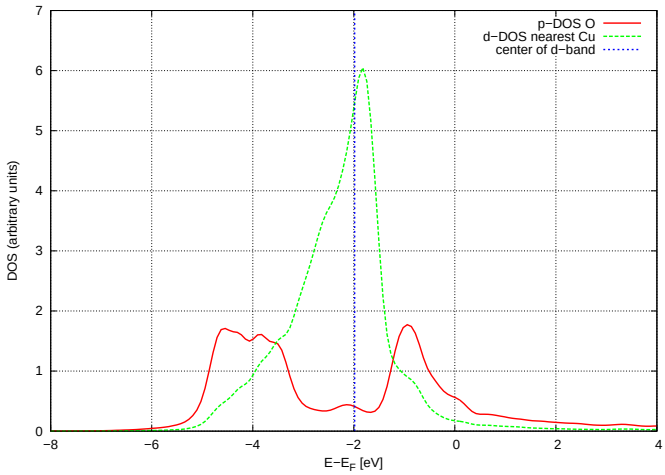

Figure 13: Projected p-DOS for the oxygen atom adsorbed on the site number one, and the d-DOS for the nearest Cu atom (number eight) on the surface.

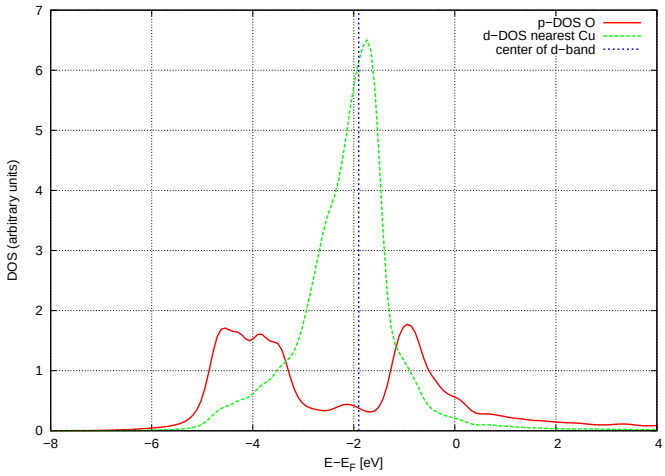

Figure 14: Projected p-DOS for the oxygen atom adsorbed on the site number one, and the d-DOS for the second nearest Cu atom (number one) on the surface.

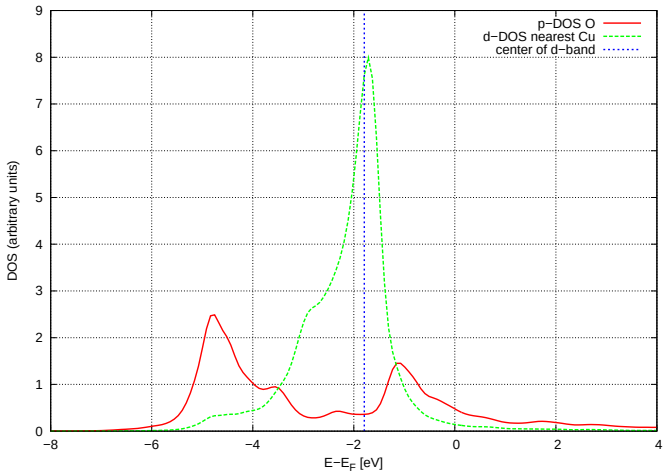

Figure 15: Projected p-DOS for the oxygen atom adsorbed on the site number two, and the d-DOS for the nearest Cu atom (number two) on the surface.

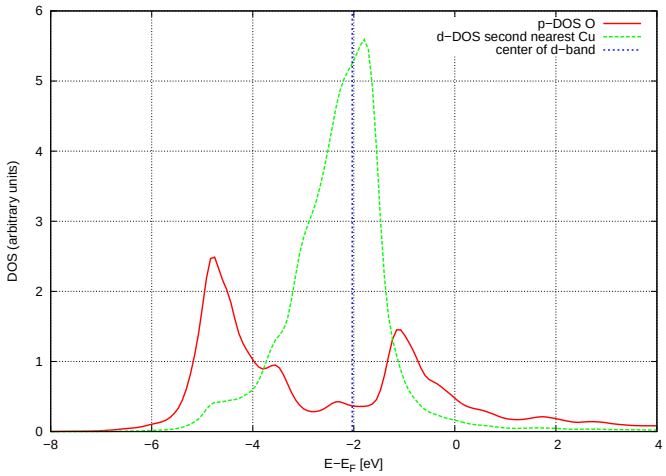

Figure 16: Projected p-DOS for the oxygen atom adsorbed on the site number two, and the d-DOS for the second nearest Cu atom (number eight) on the surface.

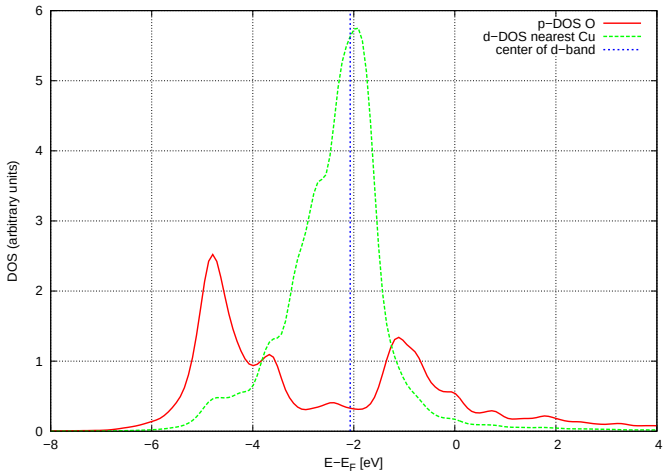

Figure 17: Projected p-DOS for the oxygen atom adsorbed on the site number four, and the d-DOS for the second nearest Cu atom (number seven) on the surface.

Based on all of the DOS figures, we can conclude that d-band structures of the Cu(510) surfaces' hollow sites are quite similar on the terrace, and the step edge causes only moderate changes on those. These results fit well on the adsorption energies calculated for the oxygen atom in previous section. The results also explain quite well why oxygen adsorption is most favourable on hollow site on terrace, and becomes slightly unfavoured on step edge and one atom row next to step edge on upper terrace, being less favoured on the foot of the step.

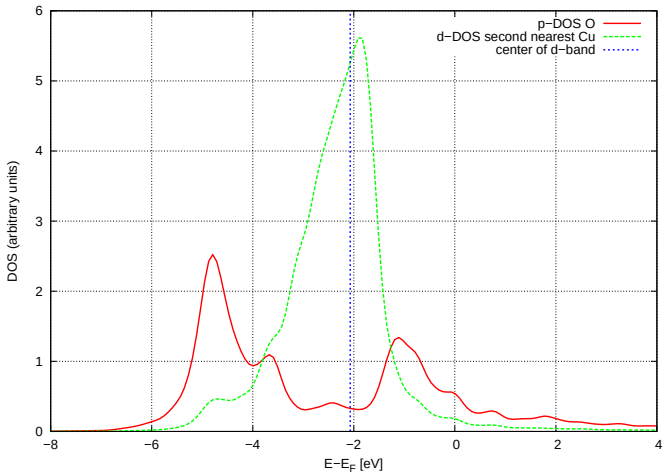

Figure 18: Projected p-DOS for the oxygen atom adsorbed on the site number four, and the d-DOS for the second nearest Cu atom (number five) on the surface.

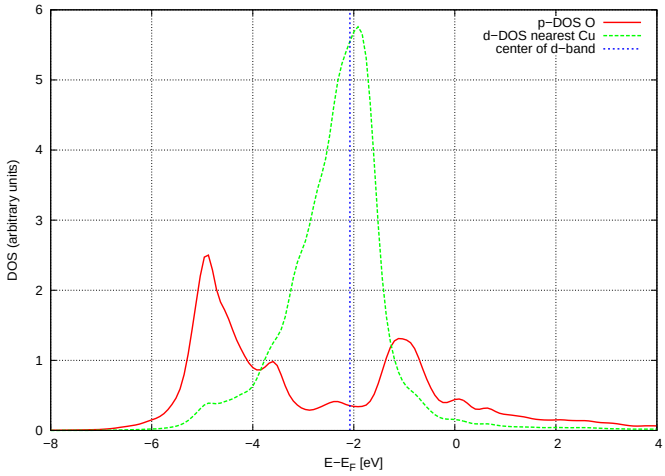

Figure 19: Projected p-DOS for the oxygen atom adsorbed on the site number 11, and the d-DOS for the nearest Cu atom (number six) on the surface.

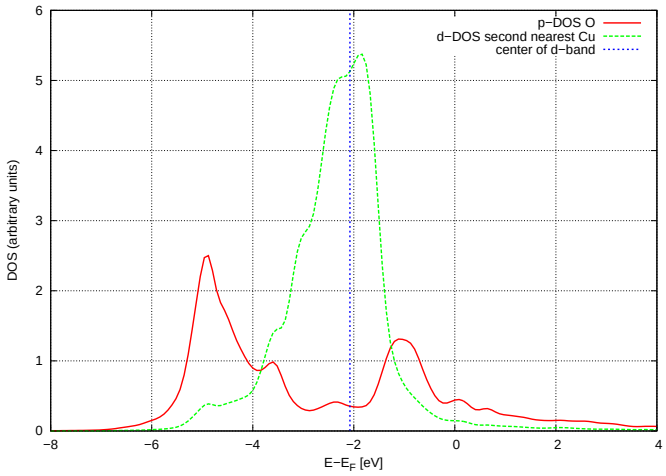

Figure 20: Projected p-DOS for the oxygen atom adsorbed on the site number 11, and the d-DOS for the second nearest Cu atom (number eight) on the surface.

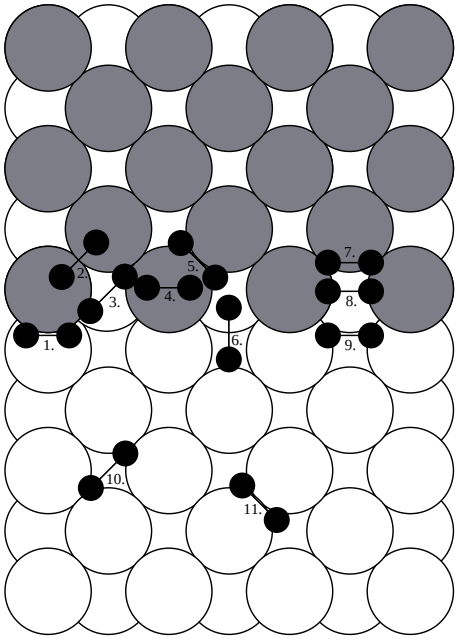

Figure 21: The selected trajectories for the molecular oxygen on the Cu(510) surface. Trajectories one, six and nine are normal to the (110) microfacet, while the rest of the trajectories are normal to (100) plane.

Table 4: Adsorption energies, E_A, and dissociation barriers, E_D, for the calculated trajectories. These values are taken directly from the data points from the calculations.

Trj.	E_A [eV]	E_D[eV]
1.	-0.08	0.38
2.	-0.44	1.83
3.	-0.68	1.06
4.	-0.18	1.45
5.	-0.11	0.20
6.	-0.17	0.63
7.	-0.30	0.40
8.	-0.40	1.44
9.	-0.61	0.12
10.	-0.94	0.57
11.	-0.10	0.21

4.4 Adsorption of molecular oxygen

After the adsorption of the atomic oxygen, the adsorption and dissociation of molecular oxygen on the Cu(510) surface was studied. These studies were limited to eleven different trajectories, from which nine are located on the step edge area, and two on the terrace. The selected trajectories are shown in figure 21. Trajectories one, six and nine are normal to (110) microfacet, and were selected to find out the PES for the microfacet. Trajectories two, three, four, five, seven and eight are on the step edge, or next to it, on the upper terrace and are normal to (100) plane. Trajectories ten and eleven are on the middle of the terrace, and are also normal to the (100) plane.

The PES for each trajectory was calculated by descending the molecule from 3.5 Å above the plane of the current adsorption site in eleven steps, and calculating the total energy of the system by a few different bonding lengths of the oxygen on each altitude. In these calculations the number of different bonding lengths was four, between 3.5 Å and 2.25 Å, and five from 2.0 Å until 1.0 Å. The total amount of energy points to be calculated was 49 for each PES figure.

After the calculation of the data points, the PES contour maps were plotted from them. The adsorption energies and dissociation barriers were also calculated directly from the absolute values of the data points, in order to minimize the error caused by fitting the contour lines in the data points. The PES elbow plots for the trajectories are shown in the figures 22 - 34, and the adsorption energies and dissociation barriers calculated from the data points are shown in Table 4.

The PES for trajectory number one is presented in figure 22. Trajectory number one is the bridge site on the (110) microfacet, where the oxygen molecule approaches the site being aligned with the step edge. This trajectory was selected for the study because the (110) hollow sites on both sides of the bridge position would potentially be attractive towards the oxygen atoms on the molecule, thus making the trajectory to be dissociative. As we can see from figure 22, this is not the case. Based on the elbow plot, on this trajectory there is no downhill in energy on the entrance channel, and also the absolute values give an adsorption energy of only -0.08 eV for this site. The dissociation is blocked by a barrier of 0.5 eV according to the elbow plot, and the absolute value for the barrier is 0.38 eV. Based on this information we can conclude that this trajectory is not favoured in molecular adsorption, because there is no attraction towards this site, and also the dissociation seems to be unlikely.

The next interesting trajectory is the number two, which is the top-bridge-top configuration on the edge of the step. The elbow plot for trajectory number two is shown in figure 23. Here we see a small downhill, which has a true value of -0.44 eV, so the 0.2 eV downhill in the upper part of the elbow plot is not true in this case. The energy minimum is located quite high, in 2.0 Å above the (100) plane, and the dissociation here is blocked by a large barrier of 1.83 eV. The trajectory number two can thus be considered to be a potential molecular adsorption site.

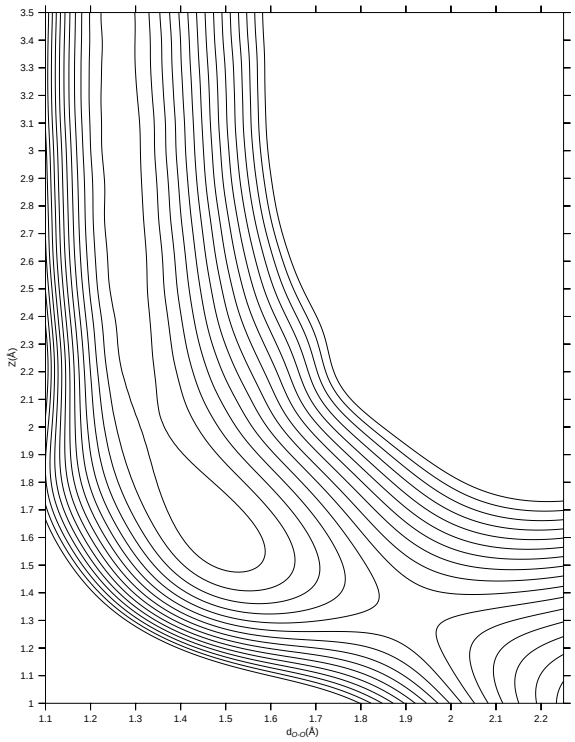

Figure 22: The PES for the oxygen molecule on trajectory number one.

In figure 24 we see the DOS for oxygen molecule in the energy minimum on trajectory number two. The copper atom nearest to O^1 is the atom number one on the step edge, and the copper atom nearest to O^2 is the atom number eight. As we can see from the figure 24 the d-band occupation of the copper atoms are enhanced by the presence of the oxygen atom, and the centers of d-band are 0.11 eV and 0.19 eV lower for the copper atoms number one and eight respectively. The p-DOS is almost identical for both oxygen atoms, and the p-DOS occupation is split to multiple peaks on different energy levels. Also the interaction and overlap between the d-states of copper and the p-states of oxygen is smaller than it was in the case of atomic adsorption on the site 11 in previous section.

Trajectory number three is the hollow site on the step edge, and here the oxygen molecule approaches the site being parallel to the (100) plane, when the intermolecular axis of the oxygen is rotated 45 degrees away from the step direction. Here we see a downhill, which has a true value of -0.68 eV, which is already bigger than it was on the previous trajectory. The dissociation is again blocked by a barrier of 1.06 eV, which is 0.77 eV smaller than it was on previous trajectory, but still enough to prevent the direct dissociation. As it was the case with the trajectory number two, the trajectory number three is also a potential molecular adsorption site.

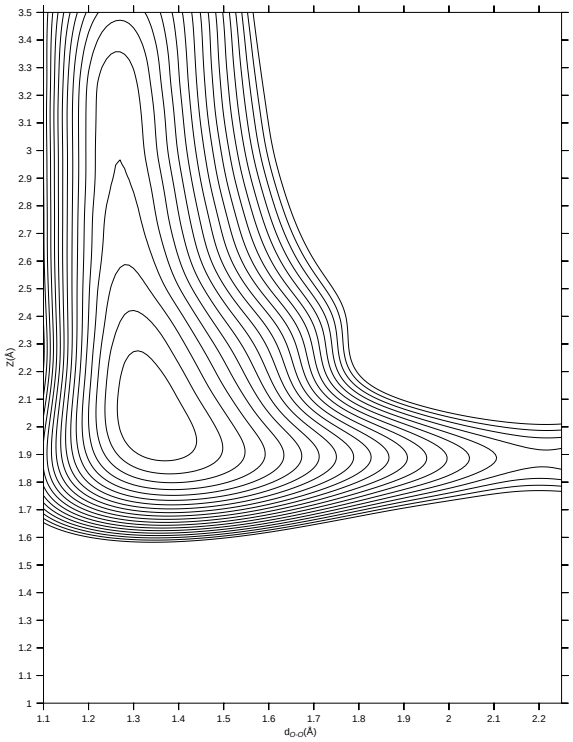

Figure 23: The PES for the oxygen molecule on trajectory number two.

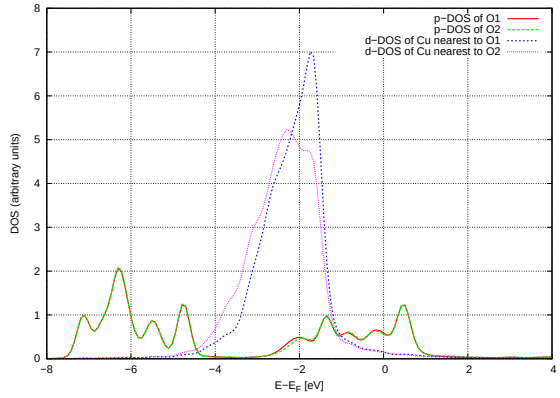

Figure 24: The DOS for oxygen molecule in the energy minimum on trajectory number two.

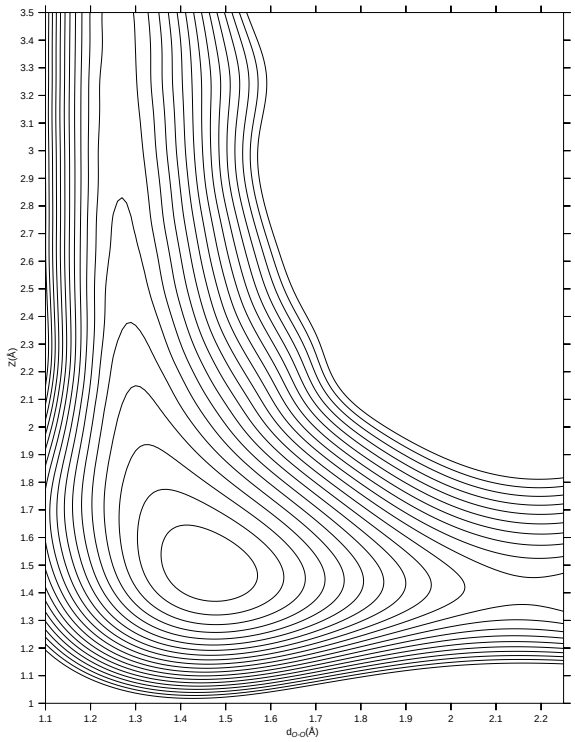

Figure 25: The PES for the oxygen molecule on trajectory number three.

In figure 26 we see the DOS for oxygen molecule in the energy minimum on the trajectory number three. In this case the copper atom nearest to O^1 is the atom number one on the step edge, and the copper atom nearest to O^2 is the atom number two on the step edge. In this case the d-band occupation of the copper atoms is also enhanced by the presence of the oxygen atom, and the centers of d-band are 0.24 eV and 0.16 eV lower for the Cu atoms number one and two respectively. The p-DOS occupation is more coherent in this case, and the occupation is enhanced on higher energy levels for the oxygen atom number one, while it is enhanced on the lower energy levels for the oxygen atom number two. Also the interaction and overlap between the d-states of copper and the p-states of oxygen is stronger than it was in the case of trajectory number two.

The PES for trajectory number four is presented in figure 27. This is the top site on the step edge atom, where the oxygen molecule is aligned along the step edge and is perpendicular to the (100) plane. Here the adsorption energy for the oxygen molecule is again only -0.18 eV, and the dissociation barrier is 1.45 eV. When we compare the PES figure for this site to those on trajectories two and three, we see that there is no barrier for oxygen to move away from this trajectory, and due to the small adsorption energy here, the oxygen molecule is very likely moved away from this place.

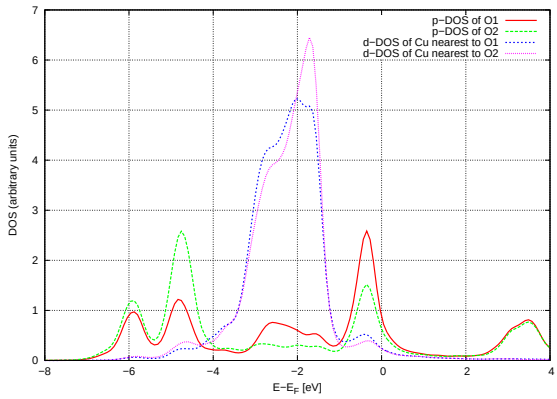

Figure 26: The DOS for oxygen molecule in the energy minimum on trajectory number three.

The PES for the oxygen molecule on the trajectory number five is presented in figure 28. Trajectory five is the same bridge site as trajectory two, but in this case the oxygen molecule is in a hollow-bridge-hollow configuration. Here the adsorption energy is once more almost non-existent -0.11 eV, but the barrier for direct dissociation is only 0.2 eV. If we compare the PES for the oxygen molecule on this trajectory to the ones on surrounding trajectories, we see that the oxygen molecule is surely moved away from this site, because there is no barrier on the way, and the neighboring site appears to be more attractive towards the oxygen.

Trajectory six on is located on the microfacet, and in this case the oxygen molecule is aligned along the missing row in the (110) structure. In this case the trajectory seems to be quite unfavoured by the oxygen atom, and this is partly due to difficulties in stretching the molecule in PES calculations without getting the other oxygen atom too close to the copper atoms on the surface. The better PES for oxygen molecule on this trajectory could be achieved by re-positioning the molecule higher from the lower terrace.

The PES for the oxygen molecule on the trajectory seven is presented in figure 30. This trajectory presents the case where the oxygen molecule approaches the step edge having both oxygen atoms on near the bridge site next to the step edge atoms. Here the oxygen molecule has the adsorption energy of -0.30 eV, and the barrier for dissociation is 0.40 eV. This trajectory would be a little bit more reactive than others, but molecular adsorption on neighboring sites is almost as favourable energetically.

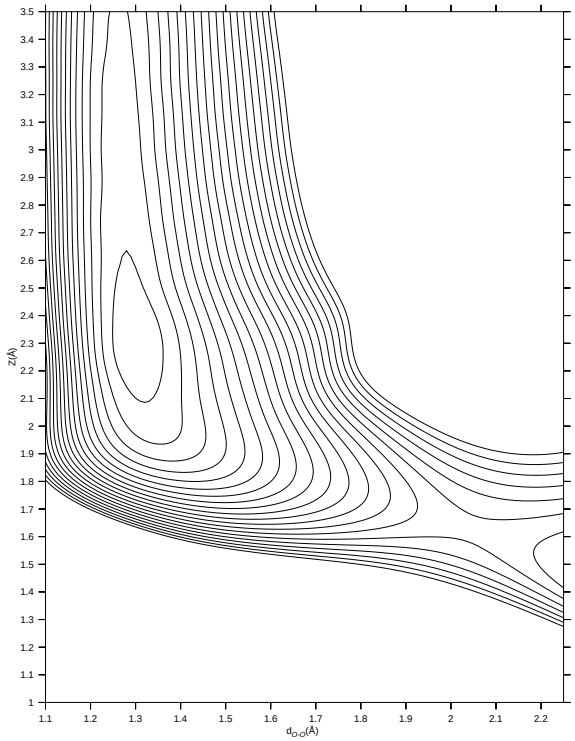

Figure 27: The PES for the oxygen molecule on trajectory number four.

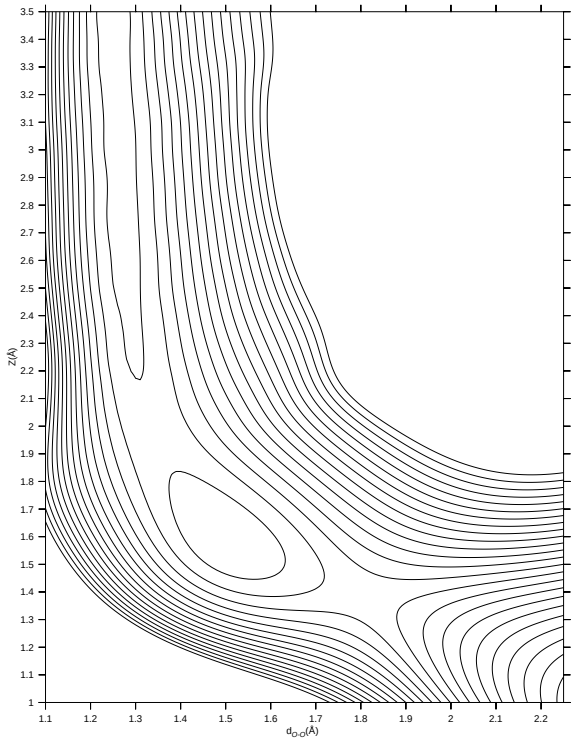

Figure 28: The PES for the oxygen molecule on trajectory number five.

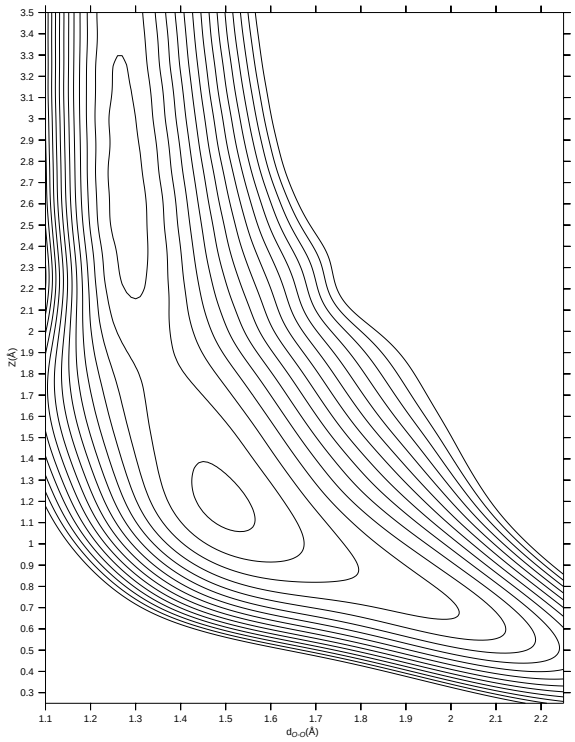

Figure 29: The PES for the oxygen molecule on trajectory number six.

Trajectory eight is almost similar to trajectory three, but here the oxygen molecule is aligned along the step edge. The PES for oxygen molecule approaching the surface on this trajectory is presented in figure 31. In this case the adsorption energy is -0.40 eV, and the barrier for dissociation is 1.44 eV. When these values are compared to those on trajectory three, we see that oxygen molecule will most likely rotate to match the trajectory three, which has -0.28 eV lower adsorption energy for oxygen molecule.

Trajectory nine presents the oxygen molecule approaching the hollow site on the (110) microfacet, being aligned along the step edge. The PES for a oxygen molecule on this trajectory is shown in figure 32. As it is clear from the figure, this trajectory is the most reactive one when it comes to the dissociation barrier, which is only 0.12 eV. The adsorption energy for oxygen molecule is -0.61 eV, so if the oxygen molecule will stay on this trajectory, it will most likely eventually dissociate here. The shape of the PES, however, indicates that there is the steric hindrance effect [38] preventing the direct dissociation.

To compare the result on the step edge to those on the terrace, also the most favourable adsorption site for atomic oxygen was studied with molecular oxygen. The PES for the molecule approaching the fourfold hollow site on the terrace, being the trajectory ten, is presented in figure 33. On this trajectory the molecule is aligned so, that both ends of

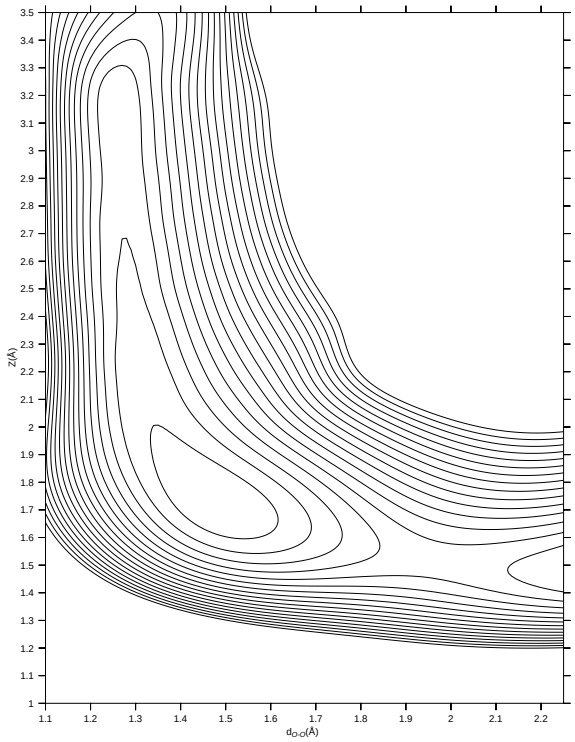

Figure 30: The PES for the oxygen molecule on trajectory number seven.

it are towards the bridge sites. As it was the case in the adsorption of atomic oxygen, this trajectory over the hollow site is also favoured by molecular oxygen. Here we get an appreciable downhill for oxygen molecule, which has an adsorption energy of -0.94 eV. On the other hand, the barrier for dissociation is 0.57, so also the dissociation is likely to occur here. The shape of the PES, however, indicates that also in this case there is the steric hindrance effect [38] preventing the direct dissociation.

The final trajectory to be studied here was the one over the bridge site on the terrace. Here the oxygen molecule approaches the surface in a similar position as on trajectory five, but here the destination is the bridge next to the fourfold hollow site, which was proven to be the most attractive one on the surface. The PES for oxygen molecule approaching the surface on this trajectory is presented in figure 34. As we can see the dissociation barrier is small, 0.21 eV, but the adsorption energy is once again very low, being only -0.1 eV. In this case it is sure, that the molecule will end up on trajectory ten, where the adsorption is much more favoured energetically.

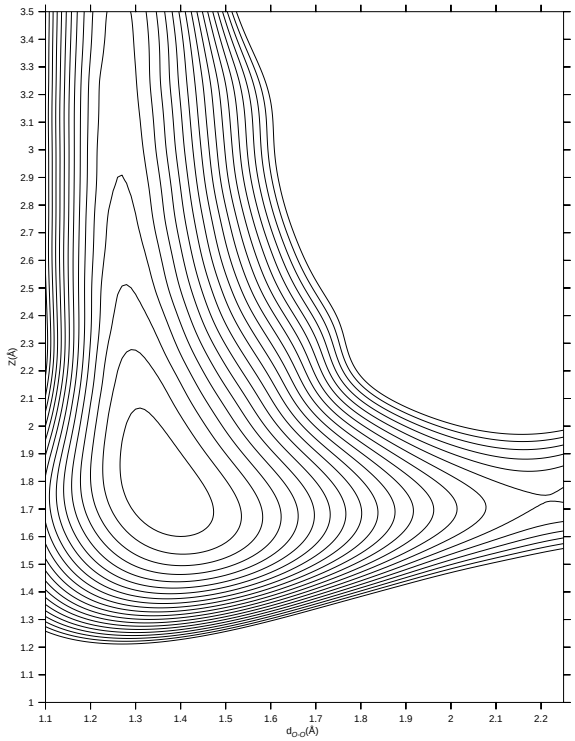

Figure 31: The PES for the oxygen molecule on trajectory number eight.

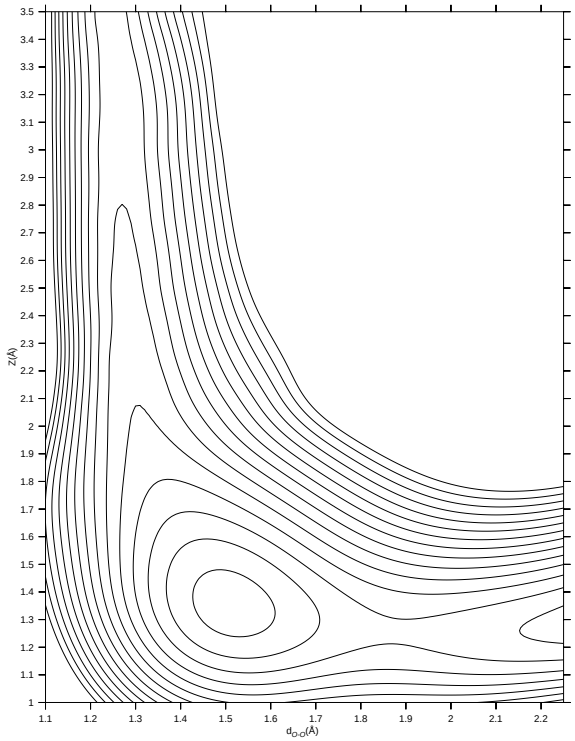

Figure 32: The PES for the oxygen molecule on trajectory number nine.

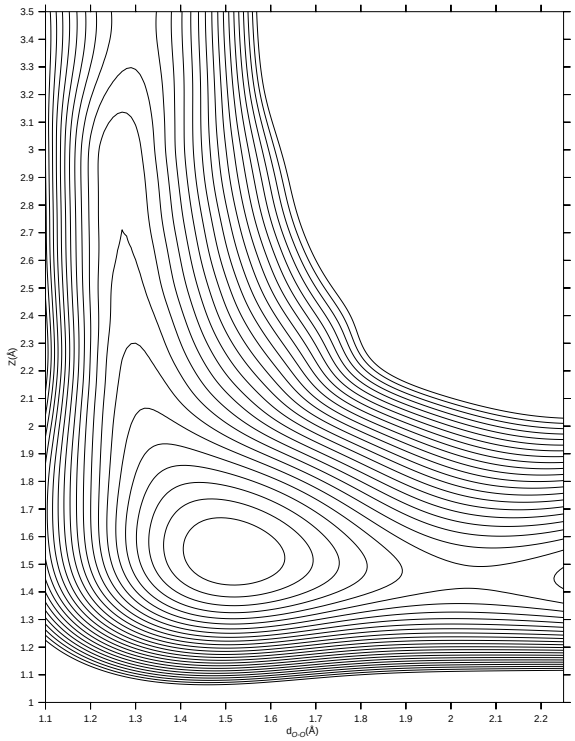

Figure 33: The PES for the oxygen molecule on trajectory number ten.

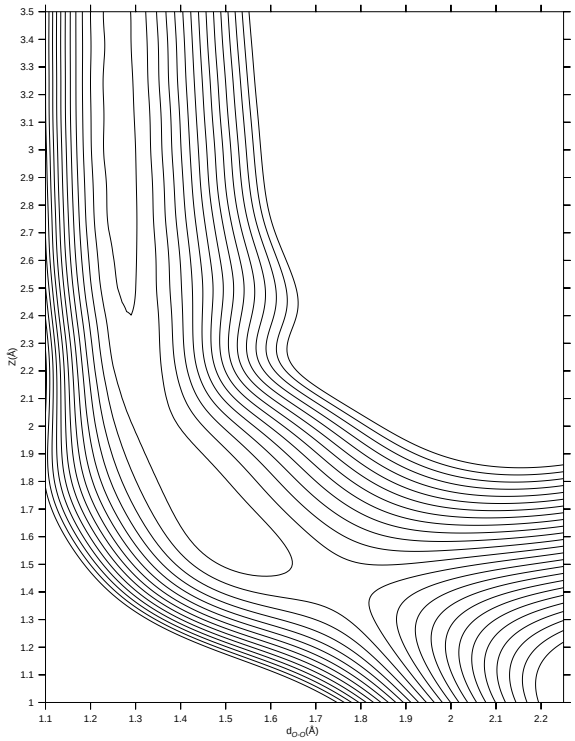

Figure 34: The PES for the oxygen molecule on trajectory number eleven.

4.5 Molecular dynamics

The PES calculations done in the previous section are static in nature, meaning that all the atoms on the surface and the oxygen molecule are held in place, and are not allowed to move during the calculations. In this way there is a risk that we miss some phenomena related to surface deformation. To make sure that there wouldn't be anything crucial missed, quantum mechanical molecular dynamics calculations were started for three trajectories on the surface. In these calculation all atoms on the system are allowed to move according to basic forces effecting between them.

In the molecular dynamics calculations the surface temperature was set to be 300 K, and it was controlled by Nosé thermostat [39], [40]. The time step used was set to be 1 fs, an the oxygen molecules were given 25 meV energy, which was directed towards the adsorption site on the surface.

The selected trajectories were trajectories number three, five and nine, and so far these calculations have already shown that the oxygen molecule does not stay on the ideal trajectories on any of the sites. In all cases the oxygen molecule first rotates in a way that its axis is almost perpendicular to the surface, and then starts to move away from the original trajectory. In the case of trajectory number nine, the oxygen molecule is steered towards the fourfold hollow site on the terrace. Also on trajectories three and five, the oxygen molecules are steered down from the step edge towards the hollow sites on the foot of the step.

By the time this thesis is written, however, these molecular dynamics are still running, and so far have not shown any signs of dissociative or molecular adsorption. What is common for all of these calculations is, that the oxygen molecule is steered close to the hollow sites, so it remains in the future to see if there exists a molecular precursor for dissociation or not.

5 CONCLUSIONS

The results for the oxygen adsorption show that the hollow sites dominate the adsorption process of the atomic oxygen on the Cu(510) surface, while adsorption on bridge and top sites remains slightly unfavoured. The adsorption of oxygen atom is 0.12 eV more favourable over the hollow site in the middle of the (100) terrace than it is on the step edge hollow site, indicating the terrace being more attractive towards the incoming oxygen. The DOS figures for the atomic oxygen also confirm the fact that copper-oxygen interaction is strongest on the (100) terrace.

As it is predicted by the adsorption of atomic oxygen, also the molecular oxygen is most likely adsorbed on terrace hollow sites according to the PES calculations. The PES calculations show a few possible molecular adsorption sites on the step edge and the terrace, the fourfold hollow site in the middle of the (100) terrace being the most favoured one, being 0.26 eV more attractive than the hollow site on the step edge. The step edge lowers the dissociation barrier by atleast 0.45 eV, and the most dissociative adsorption site is the hollow site on the (110) microfacet, where the dissociation barrier is only 0.12 eV.

What is interesting is that all the adsorption energies on the Cu(510) surface are smaller than on the smooth Cu(100) surface, and the overall reactivity of the surface is lower than was expected for a stepped surface. Also the terrace area is more attractive than step edge. This conclusion is in agreement with the results of Uesugi-Saitow and Yata [20], who concluded that the sticking process actually dominates on terraces rather than on steps or other vacant sites.

Also the molecular dynamics calculation have so far proven the terrace being more attractive towards the molecular oxygen. What it comes to the dissociativity of the Cu(510) surface being smaller than was expected, according to the PES calculations, it remains in the future results for MD calculations to see, if there exists molecular precursor for dissociative adsorption.

REFERENCES

[1] M. Hirsimäki, I. Chorkendorff, Surf. Sci. 538 (2003) 233.

[2] B. Hammer, J.K. Nørskov, Surf. Sci. 343 (1995) 211.

[3] B. Hammer, J.K. Nørskov, Nature 376 (1995) 238.

[4] P.J. Knight, S.M. Driver, D.P. Woodruff, Chem. Phys. Lett. 259 (1996) 503.

[5] M. Lahti, N. Nivalainen, A.Puisto, M. Alatalo, Surf. Sci. doi:10.1016/j.susc.2007.04.052 (2007).

[6] L. Vattuone, L. Savio, A. Gerbi, M. Okada, K. Moritani, M. Rocca, J. Phys. Chem. B 111 (2007) 1679-1683.

[7] C. Cohen, A. L'Hoir, J. Moulin, D. Schmaus, M. Sotto, J.-L. Domange, J.-C. Boulliard, Surf. Sci. 339 (1995) 41.

[8] M. Hirsimäki, private communication (2006)

[9] N.W. Ashcroft, N.D. Mermin: Solid State Physics, Thomson Learning, USA (1976).

[10] A. Groß: Theoretical Surface Science, A Microscopic Perspective, Springer, Germany (2003).

[11] D. Spišák, Surf. Sci. 489 (2001) 151.

[12] Juarez L. F. Da Silva, K. Schroeder, S. Blügel, Phys. Rev. B 70 245432 (2004).

[13] Y. Xu, M. Mavrikakis, Surf. Sci. 538 (2003) 219.

[14] D.A. Walko, I. K. Robinson, Phys. Rev. B 59 (1999) 15446.

[15] S. Dahl, A. Logadottir, R. C. Egenberg, J. H. Larsen, I. Chorkendorff, E. Törnqvist, J. K. Nørskv, Phys. Rev. Lett. 83 (1999) 1814.

[16] S. Dahl, E. Törnqvist, I. Chorkendorff, J. Catal. 192 (2000) 381.

[17] Šljivančanin, B. Hammer, Surf. sci. 515 (2002) 235.

[18] P. Gambardella, Ž. Šljivančanin, B. Hammer, M. Blanc, K. Kuhnke, K. Kern, Phys Rev. Lett. 87 (2001) 056103.

[19] L. Savio, L. Vattuone, M. Rocca, Phys. Rev. Lett. 87 (2001) 276101.

[20] Y. Uesugi-Saitow, M. Yata, Phys. Rev. Lett. 88 (2002) 256104.

[21] J. Hall, O. Saksager, I. Chorkendorff, Chem. Phys. Lett. 216 (1993) 413.

[22] L.H. Thomas, Proc. Cambridge Phil. Roy. Soc. 23 (1927) 542.

[23] E. Fermi, Rend. Accad. Naz. Lincei 6 (1927) 602.

[24] R.M. Martin: Electronic Structure, Basic Theory and Practical Methods, Cambridge University Press, UK (2004), 120.

[25] P.A.M. Dirac, Proc. Cambridge Phil. Roy. Soc. 26 (1930) 376.

[26] P. Hohenberg, W. Kohn, Phys. Rev. 136 (1964) B864.

[27] G.B. Bachelet, D.R. Hamann, M. Schlüter, C. Chiang, Phys. Rev. B 26 (1982) 4199.

[28] N. Troullier, J.L. Martins, Phys. Rev. B 43 (1991) 1993.

[29] N. Troullier, J.L. Martins, Phys. Rev. B 43 (1991) 8861.

[30] Siesta 2.0 User's Guide, [web document], avaible at: http://www.uam.es/departamentos/ciencias/fismateriac/siesta/, referred 18.5.2007.

[31] H.J. Monkhorst and J. D. Pack, Phys. Rev. B 13 (1976) 5188.

[32] R. Smoluchowski, Phys. Rev. 60 (1941) 661.

[33] M.W. Finnis, V. Heine, J. Phys. Chem. B 105 (1973) L37.

[34] L.E. Sutton (ed.), Supplement 1956-1959, Chemical Society, London UK, Special publication 18 (1965).

[35] A. Puisto: Oxygen adsorption on clean and oxygen precovered Cu(100), MSc. Thesis (2004).

[36] P. Atkins, J. de Paula: Atkin's Physical Chemistry, Oxford University Press, USA (2002).

[37] M. Lahti: Poisoning Effect of S on Pd Surfaces, MSc. Thesis (2005).

[38] A. Gross, A. Eichler, J. Hafner, M.J. Mehl, D.A. Papaconstantopoulos, Surf. Sci. Lett. 539 (2003) L542.

[39] S. Nosé, J. Chem. Phys. 81 (1984) 511.

[40] S. Nosé, Mol. Phys. 52 (1984) 255.